Xk-Related Protein 8 and CED-8 Promote Phosphatidylserine Exposure in Apoptotic Cells

Jun Suzuki *et al.*

Science **341**, 403 (2013);
DOI: 10.1126/science.1236758

Science (print ISSN 0036-8075; online ISSN 1095-9203) is published weekly, except the last week in December, by the American Association for the Advancement of Science, 1200 New York Avenue NW, Washington, DC 20005.

Xk-Related Protein 8 and CED-8 Promote Phosphatidylserine Exposure in Apoptotic Cells

Jun Suzuki,[1] Daniel P. Denning,[2] Eiichi Imanishi,[1] H. Robert Horvitz,[2] Shigekazu Nagata[1,3]*

A classic feature of apoptotic cells is the cell-surface exposure of phosphatidylserine (PtdSer) as an "eat me" signal for engulfment. We show that the Xk-family protein Xkr8 mediates PtdSer exposure in response to apoptotic stimuli. Mouse *Xkr8*$^{-/-}$ cells or human cancer cells in which Xkr8 expression was repressed by hypermethylation failed to expose PtdSer during apoptosis and were inefficiently engulfed by phagocytes. Xkr8 was activated directly by caspases and required a caspase-3 cleavage site for its function. CED-8, the only *Caenorhabditis elegans* Xk-family homolog, also promoted apoptotic PtdSer exposure and cell-corpse engulfment. Thus, Xk-family proteins have evolutionarily conserved roles in promoting the phagocytosis of dying cells by altering the phospholipid distribution in the plasma membrane.

Phospholipids are distributed asymmetrically between the outer and inner leaflets of plasma membranes (*1*): Phosphatidylserine (PtdSer) and phosphatidylethanolamine (PtdEtn) localize exclusively to the inner leaflet, whereas 60 to 70% of phosphatidylcholine (PtdCho) and sphingomyelin (SM) are found on the outer leaflet. This asymmetric distribution is disrupted during apoptosis, and exposed PtdSer on dying cells serves as an "eat me" signal to facilitate phagocytosis (*2*, *3*). PtdSer exposure and the more general transfer of phospholipids between the inner and outer leaflets are probably mediated by phospholipid scramblases (*1*), the identities of which are disputed (*4*).

We previously generated a mouse Ba/F3 pro-B cell line (Ba/F3-PS19) with a high level of PtdSer exposure, constructed a cDNA library (of clones >2.5 kb), and discovered TMEM16F, a transmembrane protein required for Ca^{2+}-dependent phospholipid scrambling but not apoptosis-dependent PtdSer exposure (*5*, *6*). To identify molecules that mediate apoptotic PtdSer exposure, we introduced a Ba/F3-PS19 cDNA library (of clones 1.0 to 2.5 kb) into Ba/F3 cells, serially enriched for cells with high PtdSer exposure, and established a cell line (LD-PS5-2-2) with a high level of PtdSer exposure (Fig. 1A) (see supplementary materials and methods). LD-PS5-2-2 cells carried a cDNA encoding Xkr8, a member of the evolutionarily conserved XK protein family (*7*) (figs. S1 and S2). With the use of the programs Transmembrane Prediction (www.ch.embnet.org) and Transmembrane Hidden Markov Model (www.cbs.dtu.dk), analyses of the amino acid sequences of vertebrate Xkr8 orthologs suggested that Xkr8 contains six transmembrane regions flanked by cytosolic N and C termini (fig. S3).

We transformed mouse T cell lymphoma WR19L cells with Fas (*8*) (WR-Fas). Fas ligand (FasL) efficiently induced apoptosis of the WR-Fas cells, accompanied by caspase-3 activation and PtdSer exposure (Fig. 1B and fig. S4). The introduction of mouse Xkr8-GFP [mXkr8 fused to green fluorescent protein (GFP)], but not mTMEM16F-GFP, increased the fraction of PtdSer-exposing cells generated by FasL (Fig. 1B). The expression of m*Xkr8* short hairpin RNAs (shRNAs) in WR-Fas cells decreased the amount of the endogenous m*Xkr8* mRNA by 76 to 82% (fig. S5) and the fraction of cells with FasL-induced PdtSer-exposure (Fig. 1C), but not levels of caspase-3 activation (fig. S5). The transformation of m*Xkr8* shRNA-expressing cells with human (h)*Xkr8* cDNA, which is not recognized by the m*Xkr8* shRNAs, restored FasL-induced PdtSer exposure. hXkr8-GFP expressed in human 293T cells localized primarily to the plasma membrane (Fig. 1D), suggesting that Xkr8 functions at the cell surface to promote apoptotic PtdSer exposure.

Human PLB-985 leukemia and Raji lymphoma cells do not expose PtdSer during apoptosis (*9*, *10*). Studies using real-time reverse transcription polymerase chain reaction (RT-PCR) indicated that the amount of *Xkr8* mRNA in PLB-985 and Raji cells was 8 and 9%, respectively, of those in Namalwa cells (Fig. 2A). PLB-985 or Raji cell transformants expressing hXkr8 responded to apoptotic stimuli by exposing PtdSer (Fig. 2B). PtdSer exposure is necessary for the recognition of apoptotic cells by phagocytes

[1]Department of Medical Chemistry, Graduate School of Medicine, Kyoto University, Yoshida-Konoe, Sakyo-ku, Kyoto, Kyoto 606-8501, Japan. [2]Howard Hughes Medical Institute and Department of Biology, Massachusetts Institute of Technology, Cambridge, MA 02139, USA. [3]Core Research for Evolutional Science and Technology, Japan Science and Technology Corporation, Yoshida-Konoe, Sakyo, Kyoto 606-8501, Japan.

*Corresponding author. E-mail: snagata@mfour.med.kyoto-u.ac.jp

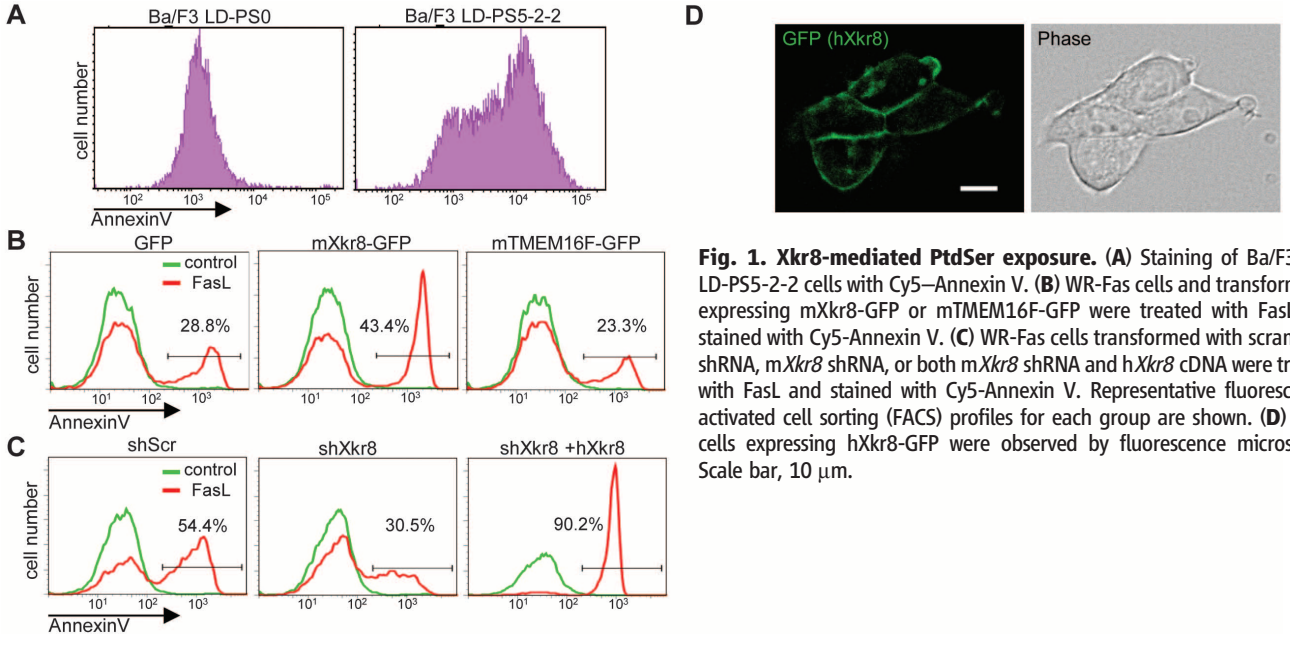

Fig. 1. Xkr8-mediated PtdSer exposure. (**A**) Staining of Ba/F3 and LD-PS5-2-2 cells with Cy5–Annexin V. (**B**) WR-Fas cells and transformants expressing mXkr8-GFP or mTMEM16F-GFP were treated with FasL and stained with Cy5-Annexin V. (**C**) WR-Fas cells transformed with scrambled shRNA, m*Xkr8* shRNA, or both m*Xkr8* shRNA and h*Xkr8* cDNA were treated with FasL and stained with Cy5-Annexin V. Representative fluorescence-activated cell sorting (FACS) profiles for each group are shown. (**D**) 293T cells expressing hXkr8-GFP were observed by fluorescence microscopy. Scale bar, 10 μm.

(*3*, *10*, *11*). Accordingly, whereas apoptotic PLB-985 cells were rarely engulfed by macrophages, their Xkr8 transformants were frequently internalized (Fig. 2C). Caspase-3 activation, DNA fragmentation, cell death, and cell shrinkage occurred similarly in PLB-985 cells with or without Xkr8 expression, indicating that Xkr8 and PtdSer exposure had no obvious effects on other aspects of the apoptotic process (fig. S6). The program CpG Island Searcher (http://cpgislands.usc.edu) identified two CpG islands near the transcription start site of the h*Xkr8* gene (fig. S7). Bisulfite DNA sequencing (*12*) indicated that none of the 23 CpGs between –232 and +4 of the h*Xkr8* gene was methylated in peripheral blood leukocyte, Jurkat, or Namalwa cells (fig. S7). By contrast, these CpGs were methylated with more than 90% probability in PLB-985 and Raji cells. Treatment of PLB-985 cells with 5-aza-2′-deoxycytidine (DAC) increased *Xkr8* mRNA levels (Fig. 2D). After 7 days of DAC treatment, all CpGs were demethylated (fig. S7), and *Xkr8* mRNA levels were 91% of that in Namalwa cells. Accordingly, DAC-treated PLB-985 cells exposed PtdSer upon ultraviolet (UV) irradiation (Fig. 2E). We suggest that the methylation of CpG islands in the *Xkr8* promoter in PLB-985 and Raji cells blocks *Xkr8* gene expression and prevents apoptotic PtdSer exposure.

We used RO09-0198 to assay staurosporine-treated, Xkr8-expressing PLB-985 cells for PtdEtn exposure, and we used 1-oleoyl-2-{6-[(7-nitro-2-1,3-benzoxadiazol-4-yl)amino]hexanoyl}-sn-glycero-3-phosphocholine (NBD-PC) and NBD-sphingosine-1-phosphocholine (NBD-SM) to assay for PtdCho and SM internalization, respectively. Inhibitor of caspase-activated DNase (ICAD) was cleaved equally well in PLB-985 and its hXkr8 transformants after staurosporine treatment (fig. S8). By contrast, apoptotic hXkr8-expressing cells (but not parental cells) stained with RO09-0198 and internalized NBD-PC and NBD-SM (fig. S8), indicating that Xkr8, like TMEM16F (*5*), promotes the scrambling of multiple lipid species. Unlike TMEM16F, Xkr8 had no effect on the Ca^{2+}-induced exposure of PtdSer (fig. S9), suggesting that distinct pathways control Ca^{2+}-induced phospholipid scrambling and apoptosis-induced scrambling. These findings are consistent with reports that B cell lines from Scott syndrome patients, who carry a null mutation in *TMEM16F*, respond to apoptotic stimuli by exposing PtdSer (*13*), and that mouse *Bak*$^{-/-}$*Bax*$^{-/-}$ platelets, which do not undergo apoptosis, expose PtdSer upon Ca^{2+} ionophore treatment (*14*).

We used the program CASVM (www.casbase.org) to analyze Xkr8 sequences from six vertebrates and, thus, identify a conserved caspase-3–recognition site near the Xkr8 C terminus (fig. S1). We generated a mutant version of hXkr8 (2DA) in which the putative caspase-recognition sequence at position 355 was changed from PDQVDG to PAQVAG (P, Pro; D, Asp; Q, Gln; V, Val; G, Gly; A, Ala) (fig. S3). PLB-985 cells expressing wild-type (WT) hXkr8-GFP exposed PtdSer in response to staurosporine (Fig. 3A), accompanied by the loss of a 52-kD hXkr8-GFP band on polyacrylamide gels and the appearance of a 29-kD band detected with antibodies to GFP (anti-GFP) (Fig. 3B). After staurosporine treatment, hXkr8(2DA)-GFP failed to promote PtdSer exposure and was not proteolytically processed; ICAD was cleaved in cells expressing either the WT or 2DA mutant of hXkr8, indicating similar caspase-3 activity in both cell lines. Processing of mXkr8-GFP at the caspase-recognition site during apoptosis was also observed in WR-Fas cells after treatment with FasL (Fig. 3C). The solubilized membrane fraction from cells expressing hXkr8-GFP was then incubated with human caspases. Western blot analysis with anti-GFP showed that caspases-3 and -7 cleaved the WT but not 2DA mutant hXkr8 (Fig. 3D). Thus, mammalian Xkr8 is activated to expose PtdSer via caspase-mediated cleavage of its cytosolic C terminus.

Mouse *Xkr8* mRNA was detectable in most mouse tissues (fig. S10), with notably high expression in the testes. We established m*Xkr8*-conditional knockout mice (fig. S11), from which we prepared mouse embryonic fibroblasts (MEFs). After treatment with staurosporine, *Xkr8*$^{+/-}$ but not *Xkr8*$^{-/-}$ MEFs exposed PtdSer (Fig. 4A). Similarly, *Xkr8*$^{flox/flox}$ and *TMEM16F*$^{-/-}$ but not *Xkr8*$^{-/-}$ fetal thymocyte (IFET) cell lines exposed PtdSer in response to FasL (Fig. 4B), although caspase-3 was activated similarly in these cell lines (fig. S12). The transformation of *Xkr8*$^{-/-}$ IFETs with mXkr8 restored PtdSer exposure in response to FasL.

The protein CED-8 is the only *Caenorhabditis elegans* homolog of Xk proteins and was previously shown to control the timing of programmed cell deaths (*15*) (fig. S2). To determine if CED-8 (like Xkr8) promotes phagocytosis, we examined *ced-8* eggs for "floater" cells, which are generated in embryos defective in engulfment; floaters are a subset of apoptotic cells that, if not engulfed (e.g., in *ced-1*, *-2*, *-5*, *-6*, *-7*, *-10*, or *-12* mutants), detach from the embryo (Fig. 4C and fig. S13) (*16*, *17*). *ced-8* eggs contained floaters, and *ced-8* mutations synergistically enhanced the number of floaters in mutants partially defective in engulfment.

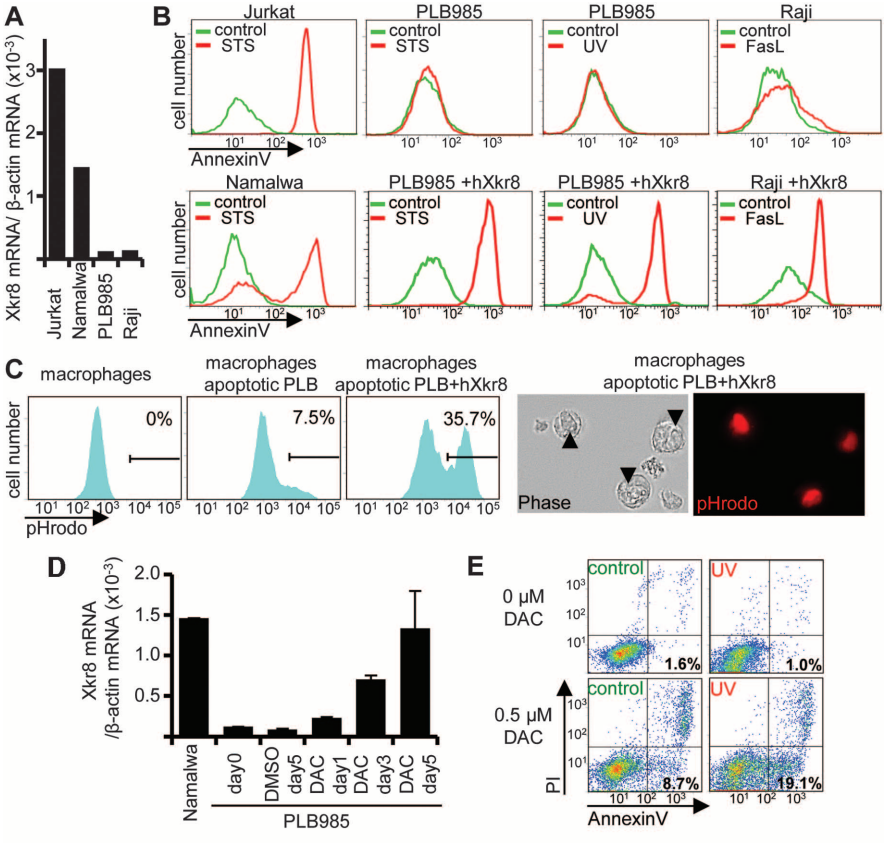

Fig. 2. Epigenetic repression of Xkr8 in human cancer cell lines. (**A**) Abundance of h*Xkr8* mRNA relative to β-*actin* mRNA was determined by real-time RT-PCR. (**B**) The indicated cell lines and hXkr8 transformants were treated with apoptotic stimuli and stained with Cy5–Annexin V. STS, staurosporine. (**C**) PLB-985 cells and hXkr8 transformants were treated with UV, labeled with pHrodo, and incubated with CD11b^{+} peritoneal macrophages. (Left) FACS profiles for pHrodo-positive CD11b^{+} cells are shown, as is the average percentage of pHrodo^{+} cells from three experiments. (Right) Macrophages (arrowheads) engulfing apoptotic cell were observed by fluorescence microscopy. (**D**) PLB-985 cells were treated with DAC, and *Xkr8* mRNA was quantified relative to *GADPH* mRNA by real-time RT-PCR. DMSO, dimethyl sulfoxide. (**E**) PLB-985 cells were treated with DAC for 5 days, exposed to UV, and stained with Cy5–Annexin V and propidium iodide.

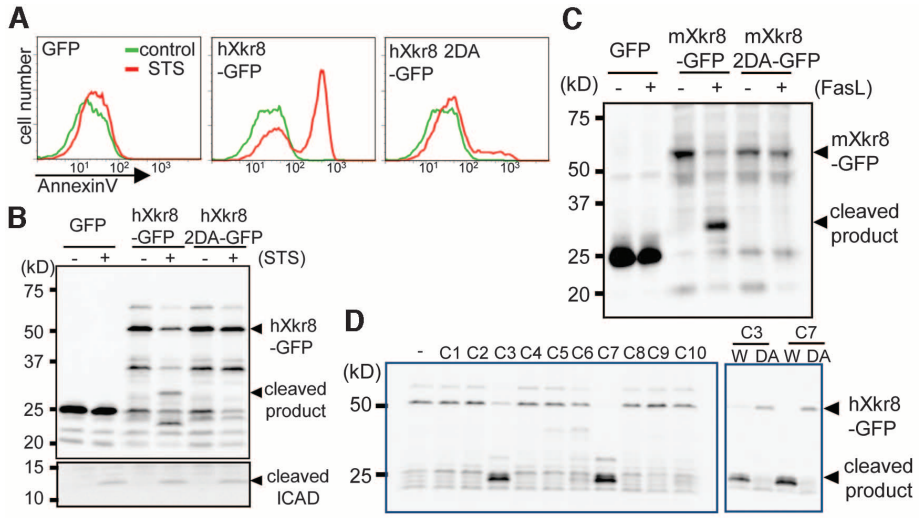

Fig. 3. Activation of Xkr8 by caspase cleavage. (**A** and **B**) PLB-985 and transformants expressing hXkr8-GFP or hXkr8 2DA-GFP were treated with STS and stained with Cy5–Annexin V (A). In (B), the cell lysates were analyzed by Western blotting with anti-GFP and anti-ICAD antibodies. (**C**) WR-Fas and transformants expressing GFP, mXkr8-GFP, or mXkr8 2DA-GFP were treated with FasL. Cell lysates were analyzed by Western blotting with anti-GFP. (**D**) The membrane fraction of PLB-985 cells expressing hXkr8-GFP (W) or the 2DA mutant (DA) was incubated with human caspases (C1 to C10, caspase-1 to caspase-10) and analyzed by Western blotting with anti-GFP antibody.

This enhancement was dependent on the caspase gene *ced-3* (fig. S14), which is required for apoptosis. The PtdSer-binding protein MFG-e8::Venus (*18*) associated with 94% of apoptotic cell corpses in the ventral cords of WT animals, but only with 21% of those in *ced-8* mutants (Fig. 4D). Similarly, PtdSer was exposed on newly detached floaters from *ced-1* but not *ced-8* or *ced-1*; *ced-8* embryos (fig. S15). Because 21% of *ced-8* ventral cord cell corpses had normal PtdSer exposure, additional factors probably contribute to this process.

In short, the Xk-related proteins Xkr8 and CED-8 promote caspase-dependent PtdSer exposure during apoptosis. Based on the following observations, Xkr8 and CED-8 probably act at a late step in PtdSer exposure, possibly in phospholipid scrambling: (i) *Xkr8*-deficient cells expose PtdSer in response to Ca^{2+}, indicating that Xkr8 is dispensable for steps before PtdSer exposure, including PtdSer biogenesis and localization; (ii) Xkr8 is directly activated by caspase cleavage, suggesting Xkr8 does not function before the onset of apoptosis; and (iii) Xkr8 and CED-8 are transmembrane proteins at the plasma membrane and, therefore, are positioned to effect, or interact with partners that effect, the externalization of PtdSer during apoptosis.

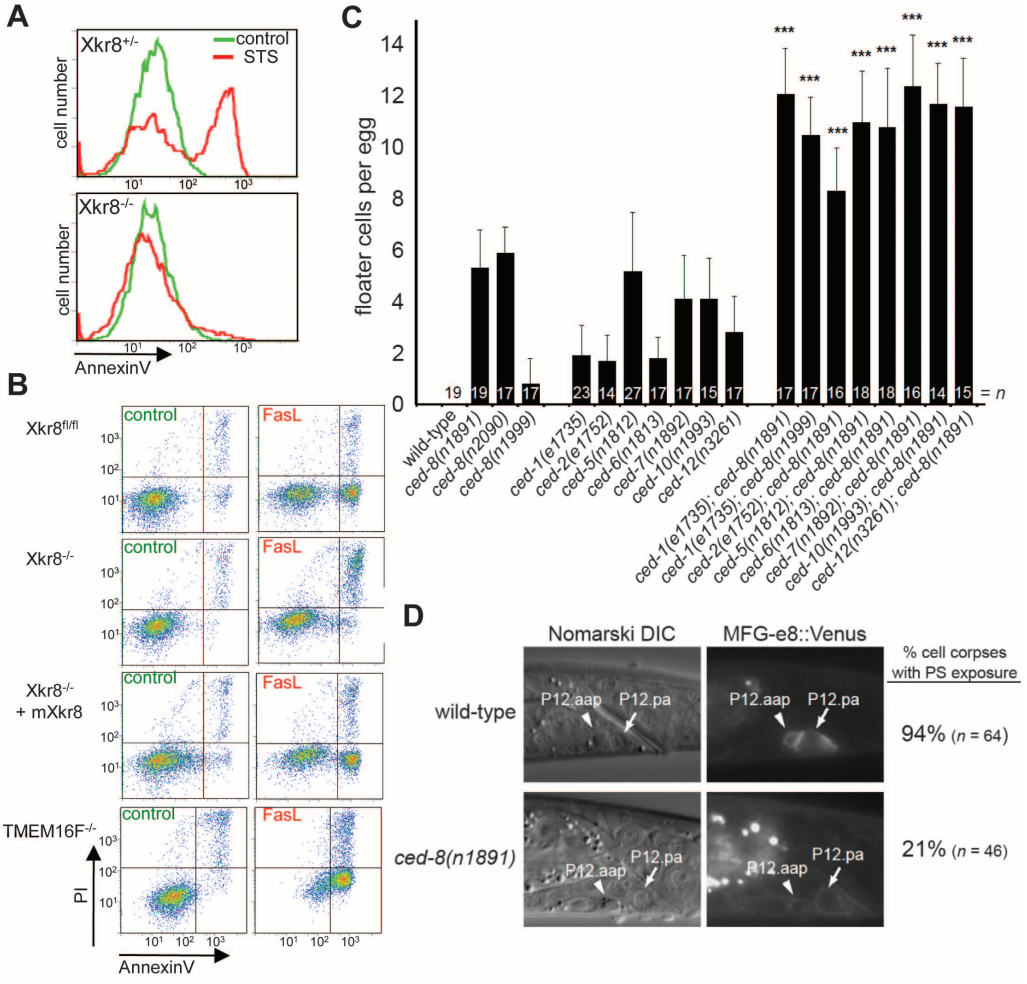

Fig. 4. Promotion of PtdSer exposure and cell-corpse engulfment by mouse Xkr8 and *C. elegans* CED-8. (**A**) MEFs from *Xkr8*$^{+/-}$ and *Xkr8*$^{-/-}$ embryos were treated with STS or control buffer for 8 hours and stained with Cy5–Annexin V. (**B**) IFETs of the indicated genotypes were treated with FasL and stained with Cy5–Annexin V and PI. (**C**) The number of floater cells per egg (n) was counted for each genotype. Error bars indicate SD. ***$P < 0.0001$ in a Student's t test for each pairwise comparison between *ced-x* and *ced-8*; *ced-x* double mutants. (**D**) PtdSer was detected using MFG-e8::Venus. Shown is the cell corpse of P12.aap (arrowhead), which undergoes apoptosis and is engulfed by P12.pa (arrow). The death of P12.aap is accompanied by PtdSer exposure in WT but not in *ced-8* (*n1891*) animals. In addition, P12.pa, like other *C. elegans* engulfing cells (*23*, *24*), exposes PtdSer on its outer plasma membrane during engulfment. DIC, differential interference contrast microscopy.

Although intracellular concentrations of Ca^{2+} increase during apoptosis (*19*, *20*), the involvement of Ca^{2+} in apoptotic PtdSer exposure is unclear (*4*), and our observations do not support a generalization. We found that FasL-induced PtdSer exposure was Ca^{2+}-dependent in WR19L cells, but not Ba/F3 cells, and that when WR19L cells were transformed with Xkr8, they lost the Ca^{2+} requirement for the apoptotic exposure of PtdSer. These results, together with the constitutive activity of overexpressed Xkr8 in Ba/F3 but not other cells, suggest that Xkr8 might cooperate with Ca^{2+}-regulated proteins in some cell-specific contexts.

The swift clearance of dead cells is essential for maintaining homeostasis, and the masking of PtdSer on apoptotic cells or the failure of the engulfment system can cause autoimmune disorders like systemic lupus erythematosus (*3*, *21*). Our finding that Xkr8 is epigenetically repressed in cancer cells suggests a mechanistic link among inflammation, autoimmunity, and cancer (*22*).

References and Notes

1. P. A. Leventis, S. Grinstein, *Annu. Rev. Biophys.* **39**, 407–427 (2010).
2. K. S. Ravichandran, U. Lorenz, *Nat. Rev. Immunol.* **7**, 964–974 (2007).
3. S. Nagata, R. Hanayama, K. Kawane, *Cell* **140**, 619–630 (2010).
4. E. M. Bevers, P. L. Williamson, *FEBS Lett.* **584**, 2724–2730 (2010).
5. J. Suzuki, M. Umeda, P. J. Sims, S. Nagata, *Nature* **468**, 834–838 (2010).
6. J. Suzuki *et al.*, *J. Biol. Chem.* **288**, 13305–13316 (2013).
7. G. Calenda *et al.*, *Gene* **370**, 6–16 (2006).
8. S. Nagata, *Cell* **88**, 355–365 (1997).
9. B. Fadeel *et al.*, *Biochem. Biophys. Res. Commun.* **266**, 504–511 (1999).
10. V. A. Fadok, A. de Cathelineau, D. L. Daleke, P. M. Henson, D. L. Bratton, *J. Biol. Chem.* **276**, 1071–1077 (2001).
11. R. Hanayama *et al.*, *Nature* **417**, 182–187 (2002).
12. J. G. Herman, J. R. Graff, S. Myöhänen, B. D. Nelkin S. B. Baylin, *Proc. Natl. Acad. Sci. U.S.A.* **93**, 9821–9826 (1996).
13. P. Williamson *et al.*, *Biochemistry* **40**, 8065–8072 (2001).
14. S. M. Schoenwaelder *et al.*, *Blood* **114**, 663–666 (2009).
15. G. M. Stanfield, H. R. Horvitz, *Mol. Cell* **5**, 423–433 (2000).
16. Y.-C. Wu, G. M. Stanfield, H. R. Horvitz, *Genes Dev.* **14**, 536–548 (2000).
17. D. P. Denning, V. Hatch, H. R. Horvitz, *Nature* **488**, 226–230 (2012).
18. V. Venegas, Z. Zhou, *Mol. Biol. Cell* **18**, 3180–3192 (2007).
19. D. L. Bratton *et al.*, *J. Biol. Chem.* **272**, 26159–26165 (1997).
20. M. B. Hampton, D. M. Vanags, M. I. Pörn-Ares, S. Orrenius, *FEBS Lett.* **399**, 277–282 (1996).
21. L. E. Muñoz, K. Lauber, M. Schiller, A. A. Manfredi, M. Herrmann, *Nat. Rev. Rheumatol.* **6**, 280–289 (2010).
22. A. L. Franks, J. E. Slansky, *Anticancer Res.* **32**, 1119–1136 (2012).
23. J. Mapes *et al.*, *Curr. Biol.* **22**, 1267–1275 (2012).
24. Y. Zhang, H. Wang, E. Kage-Nakadai, S. Mitani, X. Wang, *Curr. Biol.* **22**, 1276–1284 (2012).

Acknowledgments: We thank W. Hiraoka, M. Umeda, and M. Fujii for the PLB-985 cell line, the RO09-0198 peptide, and secretarial assistance, respectively. This work was supported in part by Grants-in-Aid for Specially Promoted Research from the Japan Society for the Promotion of Science (JSPS) to S.N., a Grant-in-Aid for Young Scientists (B) from JSPS to J.S., and postdoctoral fellowships from the Damon Runyon Cancer Research Foundation and the Charles A. King Trust to D.P.D. H.R.H. is the David H. Koch Professor of Biology at the Massachusetts Institute of Technology and is a Howard Hughes Medical Institute Investigator.

Supplementary Materials

www.sciencemag.org/cgi/content/full/science.1236758/DC1
Materials and Methods
Figs. S1 to S15
References (*25*–*44*)

19 February 2013; accepted 26 June 2013
Published online 11 July 2013;
10.1126/science.1236758

Reprogramming of Intestinal Glucose Metabolism and Glycemic Control in Rats After Gastric Bypass

Nima Saeidi,[1,2,3]* Luca Meoli,[1]* Eirini Nestoridi,[1]* Nitin K. Gupta,[1] Stephanie Kvas,[1] John Kucharczyk,[1] Ali A. Bonab,[2] Alan J. Fischman,[2] Martin L. Yarmush,[2,3] Nicholas Stylopoulos[1]†

The resolution of type 2 diabetes after Roux-en-Y gastric bypass (RYGB) attests to the important role of the gastrointestinal tract in glucose homeostasis. Previous studies in RYGB-treated rats have shown that the Roux limb displays hyperplasia and hypertrophy. Here, we report that the Roux limb of RYGB-treated rats exhibits reprogramming of intestinal glucose metabolism to meet its increased bioenergetic demands; glucose transporter-1 is up-regulated, basolateral glucose uptake is enhanced, aerobic glycolysis is augmented, and glucose is directed toward metabolic pathways that support tissue growth. We show that reprogramming of intestinal glucose metabolism is triggered by the exposure of the Roux limb to undigested nutrients. We demonstrate by positron emission tomography–computed tomography scanning and biodistribution analysis using 2-deoxy-2-[18F]fluoro-D-glucose that reprogramming of intestinal glucose metabolism renders the intestine a major tissue for glucose disposal, contributing to the improvement in glycemic control after RYGB.

Roux-en-Y gastric bypass (RYGB) induces substantial and sustained weight loss and is a highly effective treatment for severe obesity (*1*–*3*). The results of three recent prospective studies suggest that RYGB is the best treatment option for obesity-related diabetes (*4*–*6*). Interestingly, the improvement in glucose homeostasis occurs early after the RYGB procedure, before any appreciable weight loss, and patients are often able to discontinue their antidiabetic medications before hospital discharge (*4*, *5*, *7*, *8*). The precise mechanisms underlying the resolution of diabetes after RYGB have not been determined (*3*, *8*–*10*).

Several studies in rodents and one study in humans have previously described that the Roux limb displays morphological changes, characterized by hypertrophy and hyperplasia after RYGB (*11*–*16*). However, the importance of the morphological adaptation of the Roux limb, in itself, in the metabolic effects of RYGB remains largely unknown. Because the construction of the Roux limb is one of the fundamental components of the RYGB procedure (Fig. 1A) (*17*, *18*), we hypothesized that the beneficial effect of RYGB on glucose homeostasis may stem from changes in the metabolism within this reconfigured jejunal segment to meet the increased bioenergetic demands of tissue growth and maintenance, possibly in response to its exposure to undigested nutrients. To study the Roux limb, we performed RYGB in rats (*19*). RYGB led to substantial and sustained weight loss and improvement in glucose metabolism in diet-induced obese (DIO) rats, recapitulating the effects observed in humans (fig. S1, A to E). RYGB also improved glycemic control in two nonobese, diabetic rodent models with impaired insulin secretion: streptozotocin (STZ)–induced diabetic and Goto-Kakizaki (GK) rats (Fig. 1, B to D, and fig. S1, F to I). We also observed intestinal remodeling, characterized by increased intestinal mass due to hyperplasia and hypertrophy, in the Roux limb of RYGB-treated rats (figs. S2 to S4 and supplementary text 1).

To test our hypothesis, we initially sought to identify possible metabolic changes in the Roux limb of RYGB-treated rats. We compared its metabolic profile with the profile of corresponding segments of the jejunum of sham-operated rats, using a quantitative polar metabolomic profiling platform. The metabolomic profiling showed increased concentrations of glucose-6-phosphate, d-gluconate, 6-phospho-d-gluconate and nicotinamide adenine dinucleotide phosphate ($NADP^+$) in the Roux limb, suggesting that the oxidative phase of the pentose phosphate pathway (PPP) is stimulated (fig. S5, A and B, and table S1). The changes in the metabolites of the nonoxidative phase of the PPP did not reach statistical significance,

[1]Center for Basic and Translational Obesity Research, Division of Endocrinology, Boston Children's Hospital, Harvard Medical School, Boston, MA 02115, USA. [2]Shriners Hospital for Children, Boston, MA 02114, USA. [3]Center for Engineering in Medicine, Massachusetts General Hospital, Harvard Medical School, Boston, MA 02114, USA.

*These authors contributed equally to this work.
†Corresponding author. E-mail: Nicholas.Stylopoulos@childrens.harvard.edu

www.sciencemag.org/cgi/content/full/science.1236758/DC1

Supplementary Materials for

Xk-Related Protein 8 and CED-8 Promote Phosphatidylserine Exposure in Apoptotic Cells

Jun Suzuki, Daniel P. Denning, Eiichi Imanishi, H. Robert Horvitz, Shigekazu Nagata*

*Corresponding author. E-mail: snagata@mfour.med.kyoto-u.ac.jp

Published 11 July 2013 on *Science* Express
DOI: 10.1126/science.1236758

This PDF file includes:

Materials and Methods

Cell Lines, Recombinant Proteins, Antibodies, and Materials

Mouse interleukin-3 (IL-3)-dependent Ba/F3 cells (*25*) were maintained in RPMI-10% fetal calf serum (FCS, Gibco), 45 units/ml mouse IL-3, and 50 μM β-mercaptoethanol. Human PLB-985 (*26*), Jurkat, Namalwa, and Raji cells were grown in RPMI1640-10% FCS and 50 μM β-mercaptoethanol. Plat-E packaging cells (*27*) were grown in DMEM-10% FCS. Mouse IL-3 (*28*), and human FasL (*29*) were prepared as described. Rabbit anti-activated caspase-3 mAb was from Cell Signaling. Mouse anti-human ICAD mAb was from Medical & Biological Laboratories, and Alexa 488-labeled goat anti-rabbit IgG Abs were from Invitrogen. Staurosporine was provided by Kyowa Hakko Kirin.

Construction of the cDNA Library, and Identification of Xkr8

Using poly(A) RNA from Ba/F3-PS19 cells, cDNA was synthesized with random hexamers as primers, and a *Bst*XI adaptor was attached as described (*5*). DNA fragments 1.0 to 2.5 kb in length were size-fractionated by electrophoresis through a 1% agarose gel and ligated into a *Bst*XI-digested pMXs vector (*30*). Approximately 1.3 x 10^6 clones were produced with *E. coli* DH10B cells (ElectroMax DH10B; Invitrogen) by electroporation. Using plasmid DNA from the cDNA library, retrovirus was produced in Plat-E cells, concentrated by centrifugation, and used to infect Ba/F3 cells as described (*5*). Cells treated with A23187 were stained on ice for 15 min with Cy5-Annexin V (Biovision) and for 2 min with 5 μg/ml Propidium Iodide, and sorted with a FACSAria (BD Biosciences). The cDNA integrated into the retroviral vector was identified by PCR (*5*) as the Xkr8 cDNA. Real-time PCR indicated that the amount of Xkr8 mRNA in Ba/F3-PS19 is similar to that in the parental Ba/F3 cells, suggesting that the strong PtdSer exposure in Ba/F3-PS19 cells is due to the mutation introduced into TMEM16F gene (*5*).

Expression Plasmids for Mouse and Human Xkr8, and Their Mutants

The coding sequences for m*Xkr8* (GenBank NM_201368) and h*Xkr8* (GenBank NM_018053) were prepared by RT-PCR from Ba/F3 and Namalwa cells, respectively. The pMXs puro c-GFP was constructed by inserting the GFP sequence into pMXs puro. The *Xkr8* cDNAs were then inserted into pMXs puro c-FLAG (*5*) or pMXs puro c-GFP to express proteins tagged with FLAG or GFP at the C-terminus. To generate the D351A/D354A (2DA) mutant of m*Xkr8*, and the D352A/D355A (2DA) mutant of h*Xkr8*, the mouse and human *Xkr8* cDNAs were mutated by recombinant PCR (*31*) using primers carrying the mutated nucleotides.

Primers used to prepare the m*Xkr*8 and h*Xkr*8 cDNA were as follows (in each primer, the *Bam*HI or *Eco*RI recognition sequence is underlined): m*Xkr8*, 5'-ATATGGATCCATCATGCCTCTGTCCGTGCACCA-3' and 5'-ATATGAATTCGAGGACTCCATTCAGCTGCA-3'; h*Xkr8*, 5'-ATATGGATCCGCCATGCCCTGGTCGTCCCGCGG-3' and 5'-ATATGAATTCTCCCTTCACTGGCGAAGCAG-3'. Primers used to generate the D351A/D354A (2DA) mutants of m*Xkr8*, and the D352A/D355A (2DA) mutants of h*Xkr8* were : m*Xkr8* 2DA, 5'-GGGACCCTGCCCTCGTGGCTGGGACCCTAG-3', and 5'-CTAGGGTCCCAGCCACGAGGGCAGGGTCCC-3'and h*Xkr8* 2DA, 5'-AAGCCCGACCCTGCCCAGGTAGCCGGGGCC-3' and 5'-GGCCCCGGCTACCTGGGCAGGGTCGGGCTT-3'.

shRNA

Four shRNA expression plasmids for m*Xkr8* and scrambled shRNA in a pRS vector were purchased from OriGene. Among the four m*Xkr8* target sequences, the most effective was 5'-GAATCTGTGCCATCGCCTTGTTCTCAGCT-3'. WR19L cells were transfected by electroporation, and stable transformants were selected in medium with 1.0 μg/ml puromycin, and subjected to cloning by limited dilution. The *Xkr8* mRNA was quantified by real-time RT-PCR.

Establishment of *Xkr8* Knock-out Mice

Xkr8 conditionally targeted mice were generated by Unitech as a custom order. In brief, a neo-loxP cassette carrying the phosphoglycerate kinase promoter-driven neomycin-resistance gene flanked by FRT sequences was inserted into intron 3 of the *Xkr8* gene. A 1.0-kb fragment containing exon 3 was replaced with a fragment carrying the corresponding sequence and a loxP sequence. The diphtheria toxin A-fragment driven by the thymidine kinase promoter was inserted at the 5' end of the vector. Mouse Bruce-4 embryonic stem cells (*32*) were transfected with the targeting vector, and the G418-resistant clones were screened for homologous recombination by PCR. Positive clones were used to generate $Xkr8^{+/NeoFRT}$ mice, which were crossed with transgenic mice carrying cytomegalovirus enhancer-chicken b-actin hybrid promoter (CAG)-driven Cre recombinase gene (*CAG-CRE)*(*33*) or CAG-driven flippase variant *(FLPe)* gene (*CAG-FLPe*)(*34*). The resulting mice were backcrossed to the wild-type C57BL/6 to generate $Xkr8^{+/-}$ or $Xkr8^{+/flox}$ mice. Intercrosses of $Xkr8^{+/-}$ mice generated $Xkr8^{-/-}$ mice in a normal Mendelian ratio. All the mice were housed in a specific pathogen-free facility at Kyoto University, and all the animal experiments were carried out in accordance with protocols approved by Kyoto University.

Mouse Embryonic Fibroblasts and Fetal Thymocyte Cell Lines

Fibroblasts were prepared form E14.5 embryos of $Xkr8^{+/-}$ and $Xkr8^{-/-}$ mice, and cultured in DMEM containing 10% FCS. A fetal thymocyte cell line (IFET) was established by immortalizing fetal thymocytes with $H\text{-}ras^{V12}$ and *c-myc* as described (*35, 36*). In brief, $Xkr8^{+/flox}$ mice were intercrossed, and thymocytes were obtained on embryonic day 14.5. Retrovirus carrying the genes for $H\text{-}ras^{V12}$ and *c-myc* was produced in Plat-E cells with the pCX4 vector (*37*), and bound to RetroNectin-coated plates (Takara Bio) by centrifugation at 2,000 x *g* for 2-3 h. The thymocytes were attached to the retrovirus-coated plate by centrifugation at 400 x *g* for 5 min, and cultured in DMEM-10% FCS, 1 x non-essential amino acids, 10 mM Hepes- NaOH buffer (pH 7.4), 50 μM β-mercaptoethanol, 5 ng/ml mouse IL-7 (*38*) (PeproTech), and GlutaMax™ (Gibco). The resultant IFET cells were infected with Adeno-*Cre* (Adenovirus Cre/loxP, Takara Bio), and subjected to cloning by limited dilution. The $TMEM16F^{-/-}$ IFET cell line was described previously (*6*).

Transformation of Human and Mouse Cells

Retroviruses carrying a *Xkr8* cDNA were produced by introducing the pMX-puro vector into Plat-E cells, concentrated by centrifugation, and used to infect $Xkr8^{-/-}$ IFET cells. Stable transformants were selected in medium containing 2.0 μg/ml puromycin, and the expression of recombinant protein was confirmed by Western blotting with an anti-Flag Ab (Clone M2, Sigma) or anti-GFP Ab (Clone JL8, Clontech). Mouse Fas cDNA (*39*) was introduced into IFET cells by retrovirus- mediated transformation, and its expression was confirmed by flow cytometry with the anti-mouse Fas mAb (Jo2) (*40*). Human PLB-985 and mouse WR19L cells were transformed by retrovirus infection with amphotropic retrovirus envelope or VSVγ envelope. In brief, retrovirus was generated by transfecting 293T cells with the pMXs retrovirus vector, pGP (Takara Bio) for

Gag and pol-fusion protein, and pE-ampho (Takara Bio) or pCMV-VSV-G-RSV-Rev (provided by Dr. H. Miyoshi, Riken). Virus in the culture supernatant was concentrated by centrifugation and used to transform cell lines. To express Xkr8-GFP, 293T cells were transfected with pMXs puroXkr8-GFP with Fugene 6 (Promega), and transformants were selected in medium containing 1.0 μg/ml puromycin.

Induction of Apoptosis, Treatment with Ca^{2+} ionophore, and Flow Cytometry

Apoptosis was induced with FasL, staurosporine, or UV. In brief, 5 x 10^5 cells in 500 μl of medium were incubated at 37°C with 10-400 units/ml hFasL for 1.2-2.0 h or with 10 μM staurosporine for 1.5-8.0 h. For UV exposure, 1 x 10^6 cells in 2 ml of PBS were exposed to 500-2000 J/m^2 UV radiation (254 nm) in a StrataLinker (Stratagene), and incubated at 37°C for 1.5-2.0 h in 4 ml of RPMI1640-10% FCS. The cell viability was assayed by WST-1 assay with 2-(4-Iodophenyl)-3- (4-nitrophenyl)-5-(2,4-disulfophenyl)-2H-tetrazolium, monosodium salt (WST-1; Dojin Laboratories) and 1-Methoxy-5-methylphenazinium methylsulfate as described (*41*). To detect the apoptotic DNA fragmentation, DNA extracted from cells was analyzed by electrophoresis on 1.5% agarose gel. To detect active caspase-3, 1 x 10^6 cells were fixed at 37° for 10 min in PBS containing 1% paraformaldehyde, washed with chilled PBS-0.5% BSA, and permeabilized by overnight incubation at -20°C in 90% methanol. Cells in 100 μl of PBS-0.5% BSA were then incubated with 200-fold-diluted rabbit anti-active caspase-3 at room temperature for 30 min, followed by incubation for 30 min with 1,000- fold-diluted Alexa 488-labeled goat anti-rabbit IgG. The cells were washed with PBS-0.5% BSA, filtered into the FACS tube, and analyzed by a FACSAria. To monitor A23187-induced PtdSer exposure, 5 x 10^5 cells in 500 μl of Annexin V staining buffer (10 mM Hepes-NaOH buffer [pH7.4] containing 140 mM NaCl and 2.5 mM $CaCl_2$) were treated with 3.0-10 μM A23187, and analyzed with a FACSAria at 20°C.

Assay for Phospholipid Scrambling Activity

To detect phosphatidylserine (PtdSer) and phosphatidylethanolamine (PtdEtn) on the cell surface, cells were stained on ice for 15 min with 2500-5000-fold diluted Cy5-Annexin V (Biovision) or 800-fold diluted biotin-Ro09-0198 (*42*) followed by 1.0 μg/ml APC- streptavidin in Annexin V staining buffer in the presence of 5 μg/ml propidium iodide, and analyzed by a FACSAria or FACSCalibur (BD Biosciences). To assay the internalization of phosphatidylcholine (PtdCho) and sphingomyelin (SM), 1 x 10^6 cells in 0.5 ml of Hank's Balanced Salt Solution (HBSS) containing 1 mM $CaCl_2$ (HBSS-Ca) were incubated on ice for 7 min. An equal volume of 200 nM 1-oleoyl-2-{6-[(7-nitro-2-1,3- benzoxadiazol-4-yl)amino]hexanoyl}-*sn*-glycero-3-phosphocholine (NBD-PC)(Avanti Polar Lipids), or N-[6-[(7-nitro-2-1,3-benzoxadiazol-4-yl)amino]hexanoyl]-sphingosine-1- phosphocholine (NBD-SM) (Avanti Polar Lipids) in HBSS-Ca was added, and incubated at 20°C. Aliquots (150 μl) were mixed with 150 μl HBSS containing 5 μg/ml fatty-acid free BSA (Sigma-Aldrich) and 500 nM Sytoxblue (Molecular Probes), and analyzed by FACSAria.

Engulfment of Apoptotic Cells by Macrophages

Engulfment of apoptotic cells by macrophages was assayed essentially as described previously (*43*). In brief, cells were treated with UV to induce apoptosis and labeled with 0.1 μg/ml pHrodo succinimidyl ester (pHrodo, Invitrogen). Thioglycollate-elicited peritoneal macrophages were prepared from mouse peritoneal cavity 4 days after injection of 2 ml of 3% thioglycollate, and

incubated with apoptotic cells at 37°C for 2 h. The pHrodo-positive population in $CD11b^+$ macrophages was regarded as the cells engulfing apoptotic cells.

Treatment with 5-aza-2'-deoxycytidine, and Bisulfite Genomic Sequencing

To treat human PLB-985 cells with 5-aza-2'-deoxycytidine (DAC, Sigma-Aldrich), 1.0×10^6 cells in 10 ml of RPMI-10% FCS were incubated with 0.5 μM DAC for up to 7 days. Since DAC is an unstable compound, the medium was changed every 24 h. After DAC treatment, the cells were divided into three portions: one for FACS to analyze the PtdSer exposure, one for real-time RT-PCR for *Xkr8* expression, and one for methylation-specific PCR analysis (*12*). For the bisulfite genomic sequencing, DNA was modified with bisulfite using a kit (MethyEasy Xceed, Human Genetic Signatures). In brief, 3 μg DNA was denatured at 37°C for 15 min in 0.3 M NaOH, and treated with sodium bisulfite according to the protocol provided by the supplier except that the incubation time was changed to 90 min. The modified DNA was denatured at 95°C for 20 min, and amplified by PCR using primers (TTAGGGATTAGAATGTGTTT and CCTATACAAATAACCCAACT). PCR was carried out with EpiTaq HS polymerase (Takara Bio), and the product was cloned into the pGEM-Teasy vector for sequencing.

Real-time RT-PCR

Total RNA was reverse-transcribed using Superscript III reverse-transcriptase (Invitrogen) or High Capacity RNA-to-cDNA™ kit (Applied Biosystems). Specific cDNA was amplified in a reaction mixture containing LightCycler®480 SYBR Green I Master (Roche Diagnostics), and the mRNA was quantified at the point where the LightCycler System detected the upstroke of the exponential phase of PCR accumulation with the linearized plasmid DNA as reference. Primers for real-time RT-PCR were: m*Xkr8*, 5'-GCGACGCCACAGCTCACACT-3' and 5'-CCCCAGCAGCAGCAGGTTCC-3'; m*Gapdh*, 5'-AGCAGGCATCTGAGGGCCCA-3' and 5'-GAGAGCAATGCCAGCCCCGG-3'; h*Xkr8*, 5'-AGGCCGGGCCATCATCCACT-3' and 5'-TGCGCCTGTTCTGAGGCAGC-3'; and hβ-actin, 5'-GCATCCTCACCCTGAAGTAC-3' and 5'-CTTAATGTCACGCACGATTTC-3'.

Caspase Treatment of Cell Lysates

The membrane fraction was prepared from PLB-985 transformants expressing hXkr8-GFP or hXkr8 2DA-GFP as described (*28*) and solubilized in 20 mM Tris-HCl buffer (pH 7.2)-140 mM NaCl, 1% Triton X-100, 10% glycerol, and 1 mM (*p*-aminophenyl) methanesulfonyl fluoride (APMSF). After removing insoluble materials by centrifugation, the membrane proteins (20 μg) were incubated at 37°C for 1 h with 3 units of various recombinant human caspases (Biovision) in 100 μl of 50 mM Hepes-NaOH (pH 7.4), 50 mM NaCl, 5% glycerol, 5 mM DTT, 10 mM EDTA, 0.1 mM APMSF and 0.1% CHAPS, and analyzed by Western blotting.

Western Blotting

Cells were lysed in RIPA buffer (50 mM Hepes-NaOH buffer [pH 8.0], 1% NP-40, 0.1% SDS, 0.5% sodium deoxycholate, 150 mM NaCl, and 10% protease inhibitor cocktail). The lysates were mixed with 5 x SDS sample buffer (200 mM Tris-HCl [pH 6.8], 10% SDS, 25% glycerol, 5% β-mercaptoethanol, and 0.05% bromophenolblue), and incubated at room temperature for 1 h to detect Xkr8-GFP, or boiled for 5 min to detect other proteins. Proteins were separated by SDS-PAGE on a 10-20% gradient gel (Bio Craft), and transferred to a PVDF membrane (Millipore). The membranes were probed with 3000-fold-diluted mouse anti-GFP mAb, 3000-fold-diluted mouse

anti-human ICAD mAb, or 3000-fold-diluted rabbit anti-active caspase-3 mAb followed by incubation with 1,000-fold-diluted HRP-conjugated goat anti-mouse or rabbit Igs (Dako). The peroxidase activity was detected by the Western Lightning®-ECL system (PerkinElmer).

C. elegans Strains, Plasmids and Experimental Procedures

C. elegans strains were cultured as described (*44*) and maintained at 20°C. The Bristol strain N2 was used as the wild-type strain. Mutations used are listed below:

LGI: *ced-1(e1735, n2091)*.
LGIII: *ced-6(n1813)*, *ced-7(n1892)*, *ced-12(n3261)*.
LGIV: *ced-2(e1752)*, *ced-3(n3692, n2424), ced-5(n1812)*, *ced-10(n1993)*.
LGX: *ced-8(n1891, n1999, n2090), nIs106[*P_{lin-11}*::gfp]*.
unknown linkage: *nIs398[*P_{dyn-1}*::mfg-e8::Venus,* P_{myo-2}*::dsRed]*.

Shed cells or floaters were counted in eggs between the 2-fold and 3.5-fold stages of development (approximately 450–600 min after the first cell division) using a Zeiss Axioskop wide-field microscope equipped with a 100x objective equipped and Nomarski differential interference contrast (DIC) optics as described (*17*). PtdSer exposure on the corpses was detected using secreted MFG-e8::Venus expressed from the transgene *nIs398* (*18*). All images were acquired using OpenLab software (PerkinElmer) and modified for publication using ImageJ.

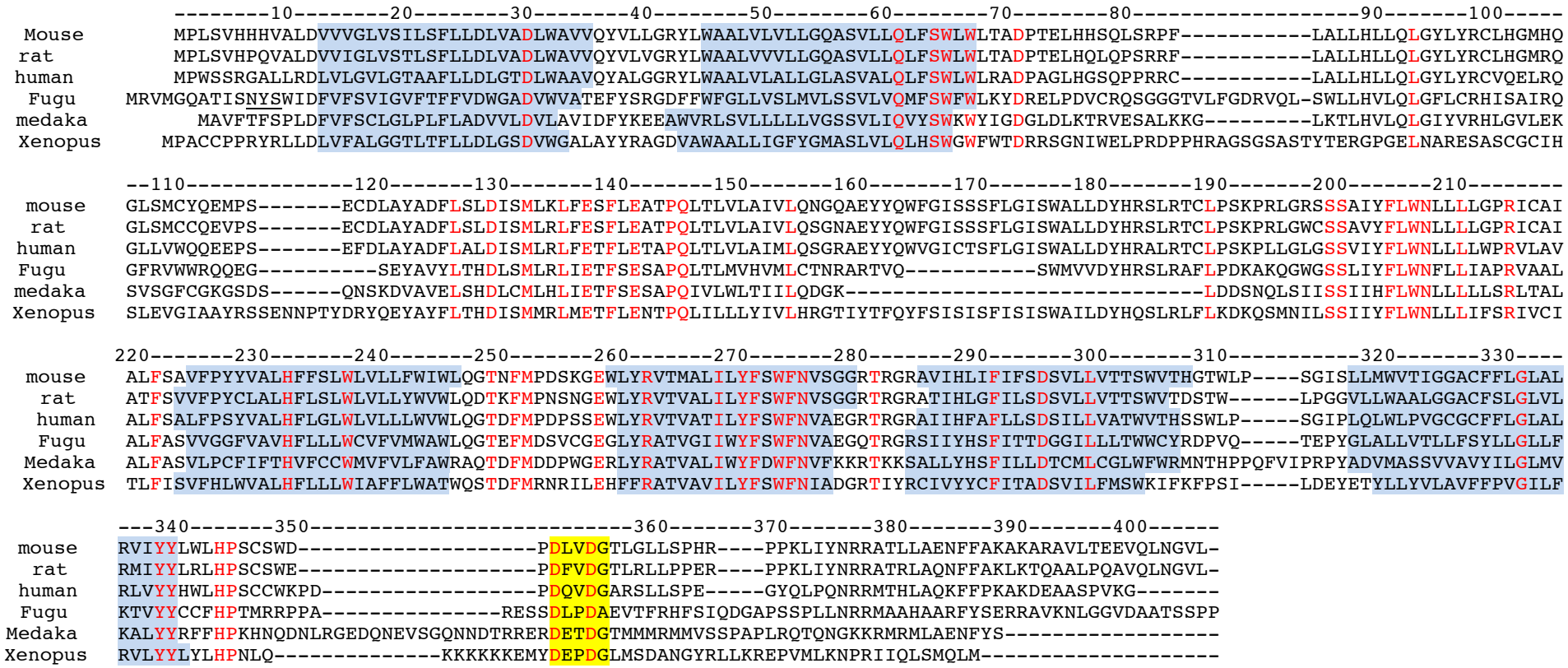

Fig. S1. An alignment of the amino acid sequences of six vertebrate Xkr8 orthologs. The putative transmembrane regions are shaded blue, perfectly conserved amino acids are red, and the caspase-recognition sites are yellow.

Fig. S2. An alignment of amino acid sequences of mouse Xkr8, *C. elegans* CED-8, and *Drosophila* CG32579. Identical amino acids are red, and similar amino acids are pink. Similar amino acids are defined as residues belonging to one of the following groups: S, T, P, A, and G; N, D, E, and Q; H, R, and K; M, I, L and V; F, Y, and W. Putative transmembrane regions are underlined, and the caspase recognition site in mouse Xkr8 is indicated in green. The number at the end of sequence indicates the number of amino acids of each protein.

A

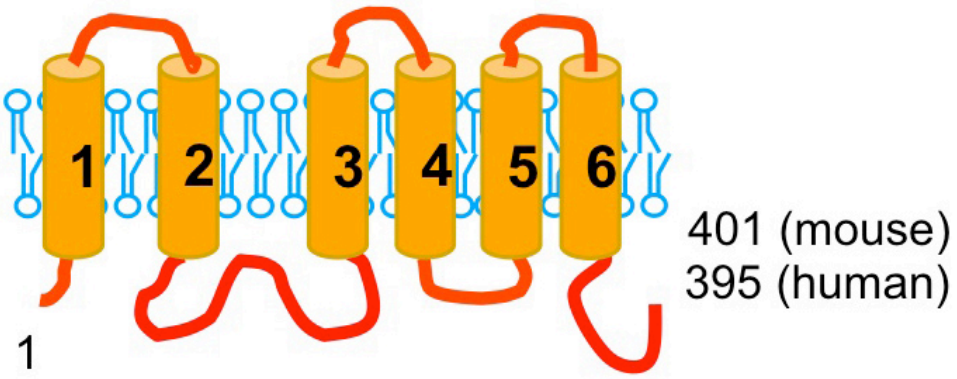

B

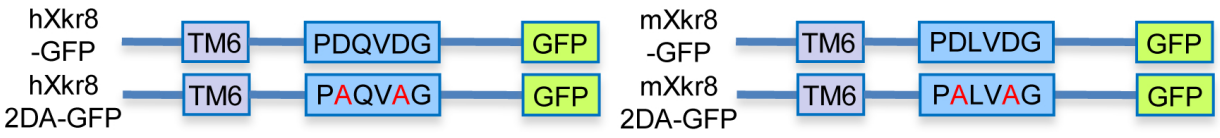

Fig. S3.

Xkr8 and its GFP-fusion proteins. (**A**) The predicted topology of mammalian Xkr8 proteins. Putative transmembrane regions are numbered. (**B**) Representations of wild-type and caspase-resistant (2DA) mutant forms of hXkr8 and mXkr8 fused to GFP. TM, transmembrane.

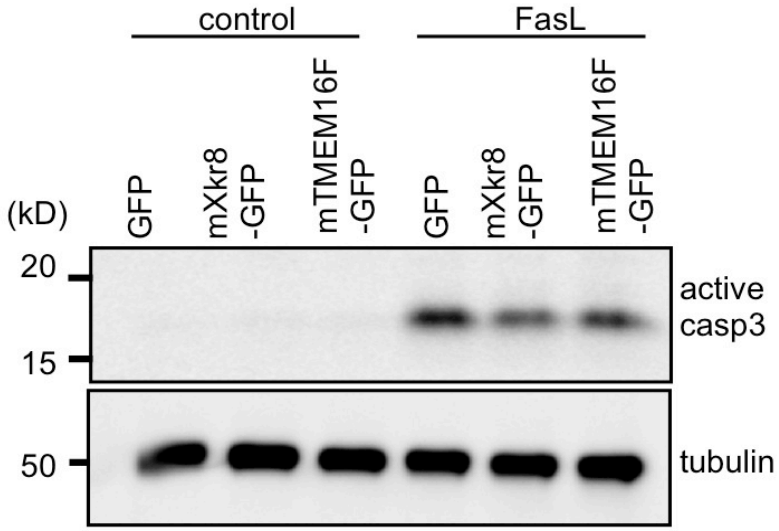

Fig. S4

FasL-induced activation of caspase-3. WR-Fas transformants expressing GFP, mXkr8-GFP or mTMEM16F-GFP were treated with FasL. The cell lysates were analyzed by western blotting with anti-active caspase-3 and anti-α-tubulin antibodies.

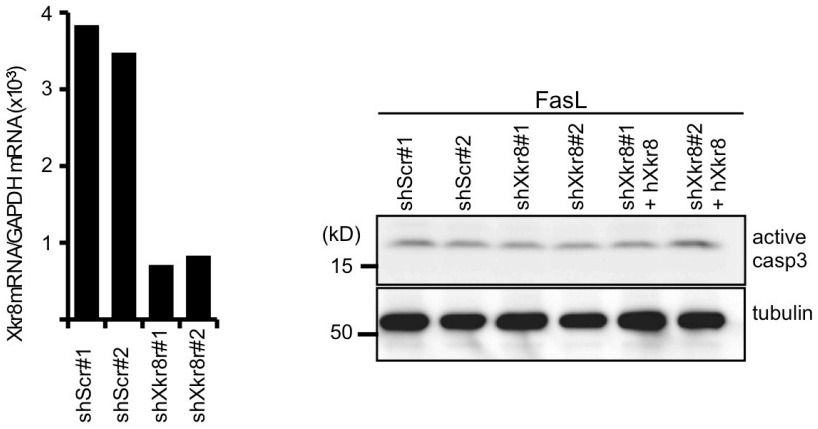

Fig. S5

Real-time PCR quantification of m*Xkr8* mRNA abundance (relative to *GAPDH* mRNA) in WR-Fas clones transformed with plasmid DNA carrying m*Xkr8* shRNA or scrambled (Scr) shRNA. Two clones for each transformant were analyzed. Right, effect of m*Xkr8*-shRNA on caspase-3 activation. For each WR-Fas transformation (Scr shRNA-expressing, m*Xkr8* shRNA-expressing, and m*Xkr8* shRNA- plus h*Xkr8*-expressing transformants), two independent samples were treated with FasL, lysed, analyzed by western blotting with anti-active caspase-3 and anti-α-tubulin antibodies.

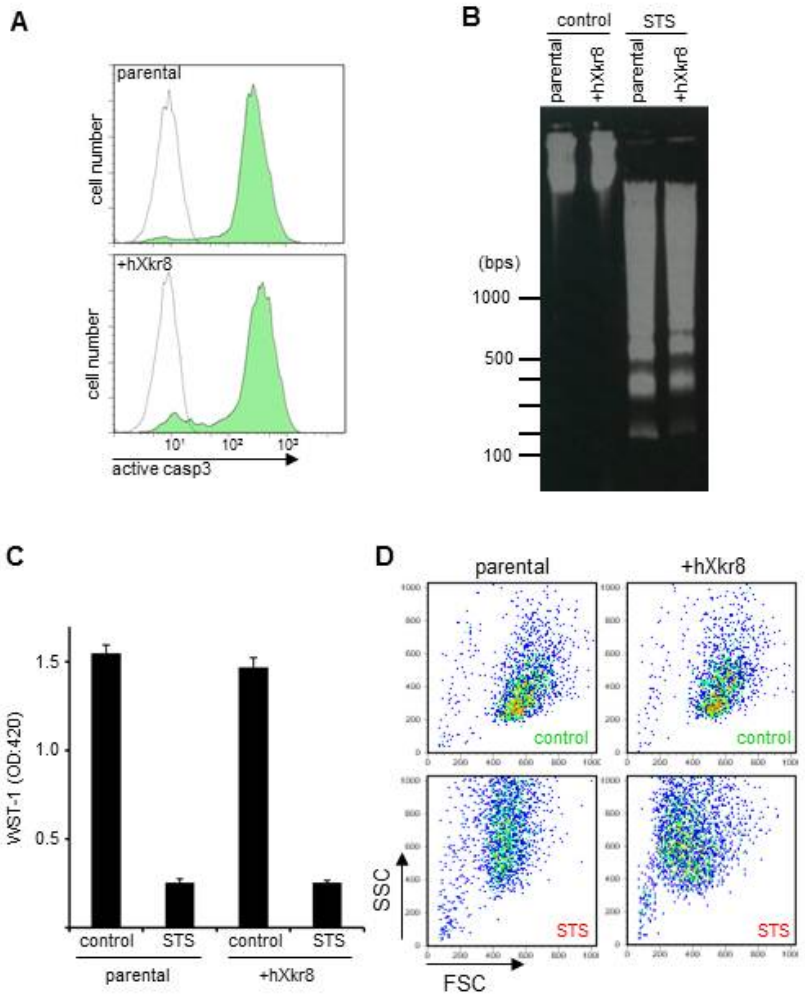

Fig. S6

Xkr8 does not affect most aspects of apoptotic cell death. Human PLB985 cells (parental) and their human *Xkr8*-transformants (+h*Xkr8*) were treated with 10 mM staurosporine (STS) for 4 hr or left untreated (control). (A) Activation of caspase-3. Paraformaldehyde-fixed cells were permeabilized by treating with methanol and stained with rabbit anti-active caspase-3. The FACS profiles of control and STS-treated cells are represented by green and open areas, respectively. (B) DNA fragmentation. DNA was prepared from control and STS-treated cells, submitted to agarose gel electrophoresis, and stained with ethidium bromide. (C) Cell death. Cell death was assayed by the WST-1 method as described in Materials and Methods. (D) Cell shrinkage. The cells were analyzed by FACSAria. The FSC profiles represent cell size.

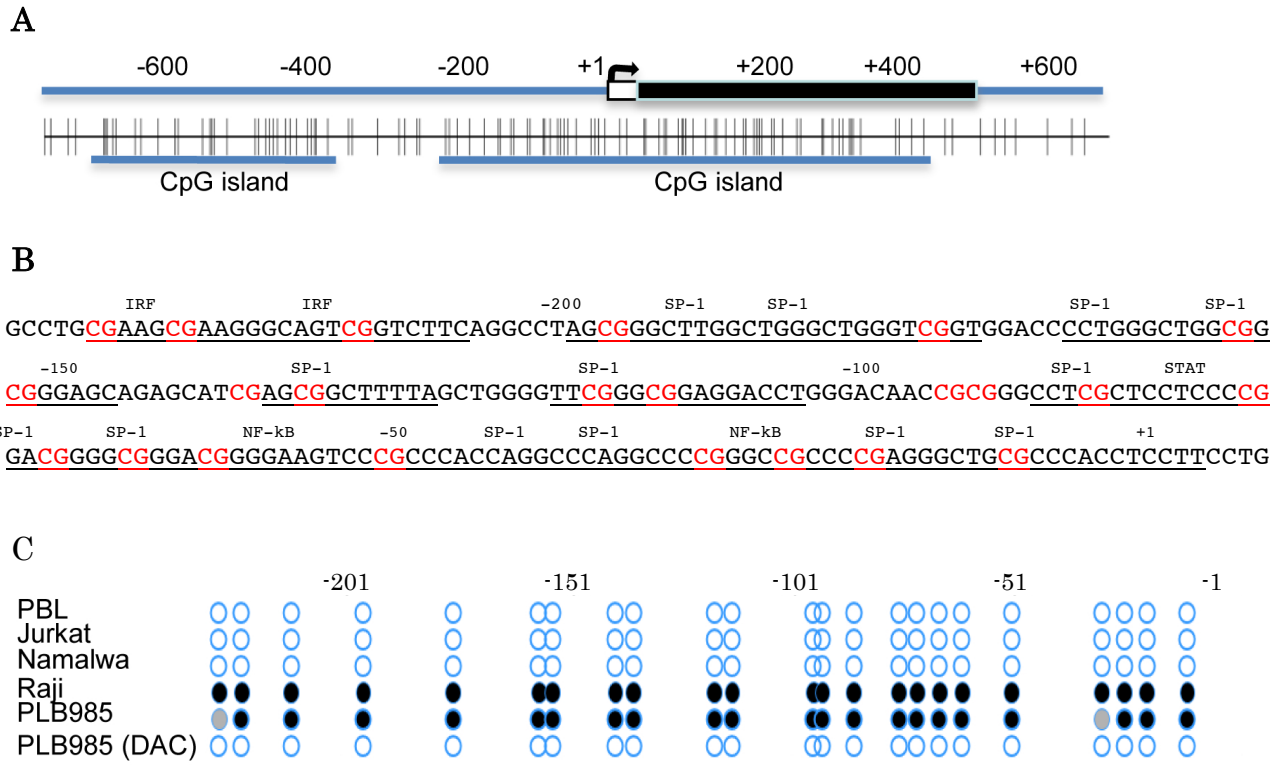

Fig. S7.

Methylation of the CpG islands in h*Xkr*8 gene. (**A**) CpG islands in h*Xkr8* gene promoter. Open and filled boxes, 5' non-coding and coding regions, respectively. Arrow, transcription start site. Each CpG is represented by a vertical bar. (**B**) The nucleotide sequence from -232 to +4 of the h*Xkr8* gene. The 23 CpGs are shown in red, and predicted transcription-factor recognition sites are underlined. (**C**) Methylation status of the CpG islands. Each circle represents a CpG between positions -232 and +4, and the extent of methylation is represented by shading: black, 76-100%; grey, 26-75%; white, 0-25%.

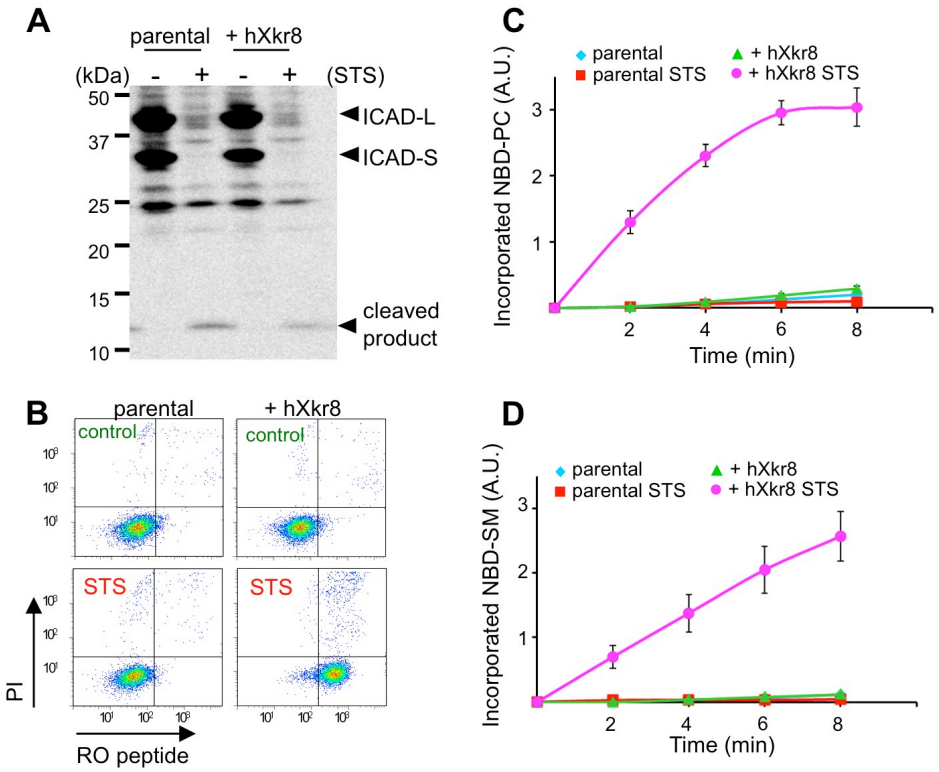

Fig. S8.

Characterization of the hXkr8-mediated scrambling of phospholipids. (A) Apoptotic cleavage of ICAD. PLB-985 cells and h*Xkr*8-expressing transformants were treated with STS, and cell lysates were analyzed by western blotting with anti-ICAD. (B) Apoptotic exposure of PtdEtn. PLB-985 and h*Xkr8*-expressing transformants were treated with STS, stained with biotin-RO peptide and streptavidin-APC and PI, and analyzed by FACS. (C and D) Scrambling of PtdCho and SM in apoptotic cells. PLB-985 and h*Xkr8*-expressing transformants were treated with STS and incubated with NBD-PC (C) or NBD-SM (D). Unincorporated lipids were extracted and analyzed by FACSAria at two minute time intervals. The fluorescence intensity in the SytoxBlue-negative fraction is shown in arbitrary units as the internalized NBD-PC or NBD-SM.

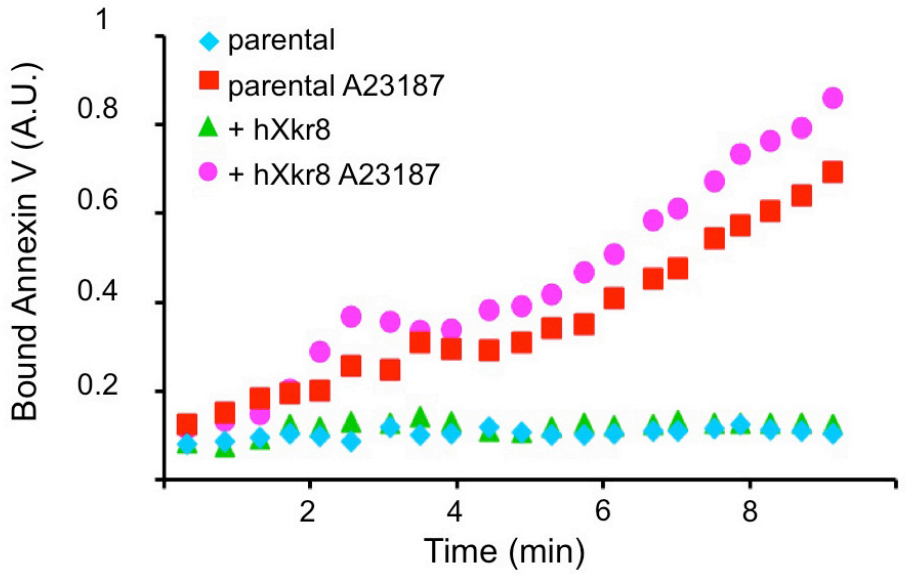

Fig. S9.

h*Xkr8* does not alter Ca^{2+}-dependent PtdSer exposure. PLB-985 and its h*Xkr8* transformants were treated at 20°C with 10 μM A23187 and stained with Cy5-labeled Annexin V. Annexin V-binding to the cells was monitored by flow cytometry at two minute intervals for 10 min.

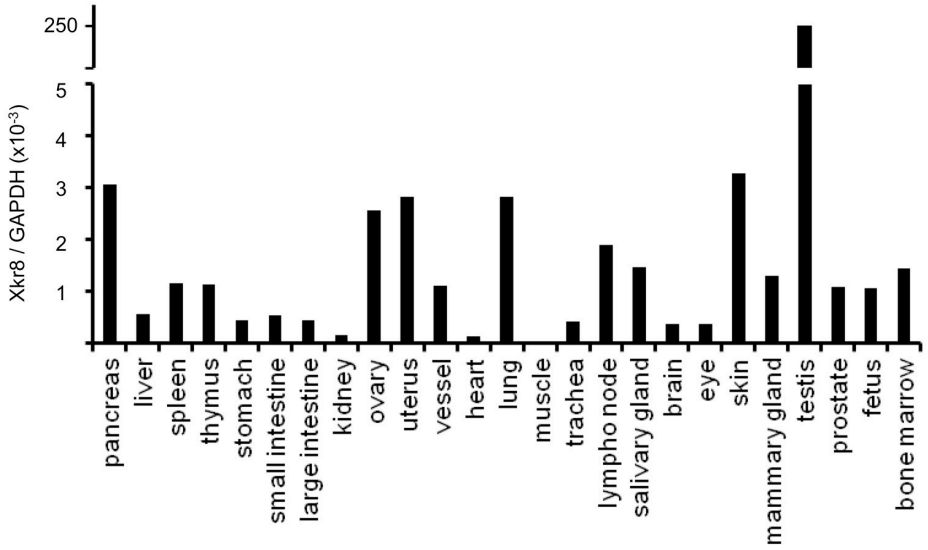

Fig. S10

Xkr8 mRNA abundance in different mouse tissues. Tissue-specific *Xkr8* mRNA levels were determined by real-time RT-PCR and expressed relative to *Gapdh* mRNA.

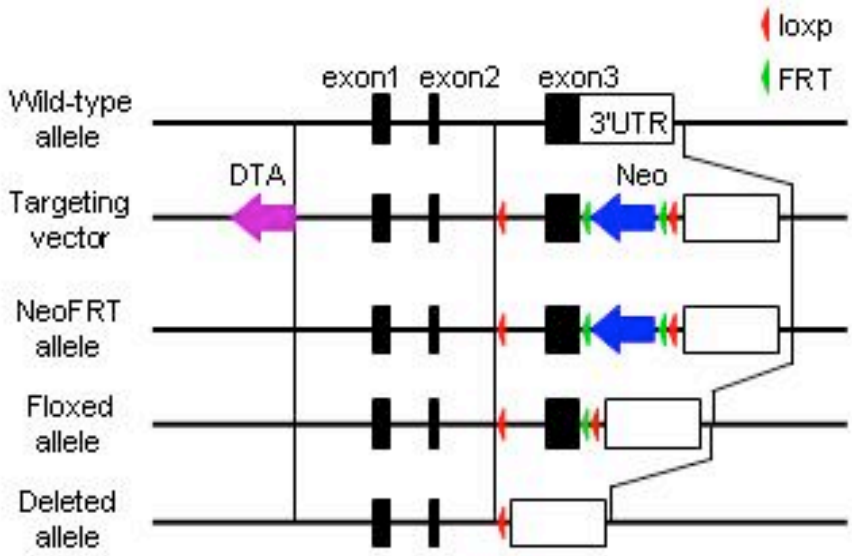

Fig. S11.

Gene structures of wild-type, floxed and deleted alleles of m*Xkr8* and the targeting vector.

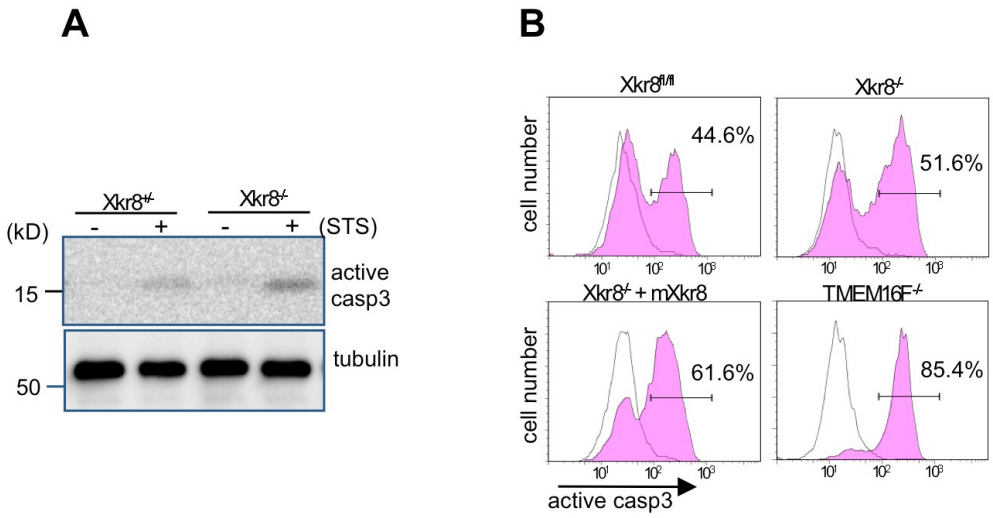

Fig. S12.

mXkr8 is not required for apoptosis-induced caspase-3 activation. (A) MEFs from *Xkr8*$^{+/-}$ and *Xkr8*$^{-/-}$ embryos were treated with (+) or without (-) staurosporine (STS) for 8 h. Cell lysates were analyzed by western blotting using anti-active caspase-3 or anti-α-tubulin antibodies. (B) The *Xkr8*$^{fl/fl}$, *Xkr8*$^{-/-}$, m*Xkr8*-transformed *Xkr8*$^{-/-}$, and *TMEM16F*$^{-/-}$ IFETs expressing Fas were treated with FasL, stained with anti-active caspase-3, and analyzed with flow cytometry. The FACS profiles for the untreated (open) and FasL-treated cells (filled) are shown. The percentage of cells carrying the active caspase-3 is indicated.

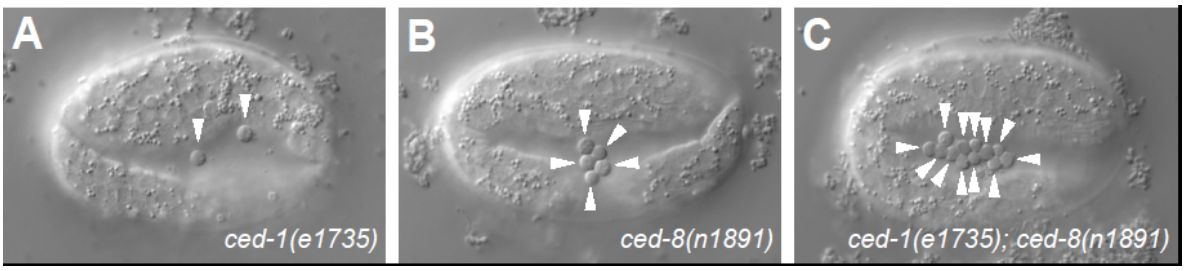

Fig. S13.

ced-8, the *C. elegans* homolog of mammalian *Xkr8*, promotes the engulfment of apoptotic cells. Shown are Nomarski DIC micrographs of (A) *ced-1(e1735)*, (B) *ced-8(n1891)*, and (C) *ced-1(e1735); ced-8(n1891)* eggs that contain unengulfed apoptotic cells (termed "floaters" and indicated by arrowheads), which have detached from the developing embryo.

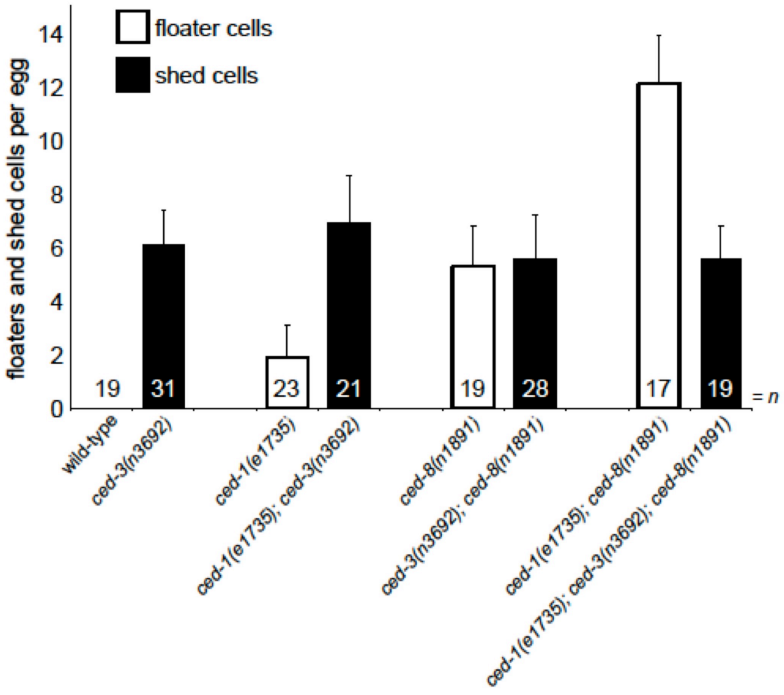

Fig. S14

The pro-apoptotic caspase CED-3 is required for the generation of floater cells in the eggs of *ced-8* mutants and other mutants defective in cell-corpse engulfment. Shown are the combined numbers of embryonic floater and shed cells that were counted in the eggs of each genotype. *ced-3* mutations cause the extrusion of shed cells (*17*). Shed cells are morphologically different from floater cells generated by mutants defective in engulfment. We observed that *ced-1* and *ced-8* mutations synergistically cause the appearance of floater cells. By contrast, *ced-3* mutations caused the appearance of shed cells and suppressed the generation of floaters in all tested genetic backgrounds, including *ced-1; ced-8*. Thus, *ced-3* is epistatic to *ced-1* and *ced-8* with respect to the generation of shed cells and the suppression of floater cells, indicating that the floater cells of *ced-1; ced-8* mutants are dependent on apoptosis. For ease of presentation, we have indicated that *ced-3* mutants generate shed cells (black bars) and that *ced-1* and *ced-8* mutants generate floaters (white bars). Error bars, standard deviations.

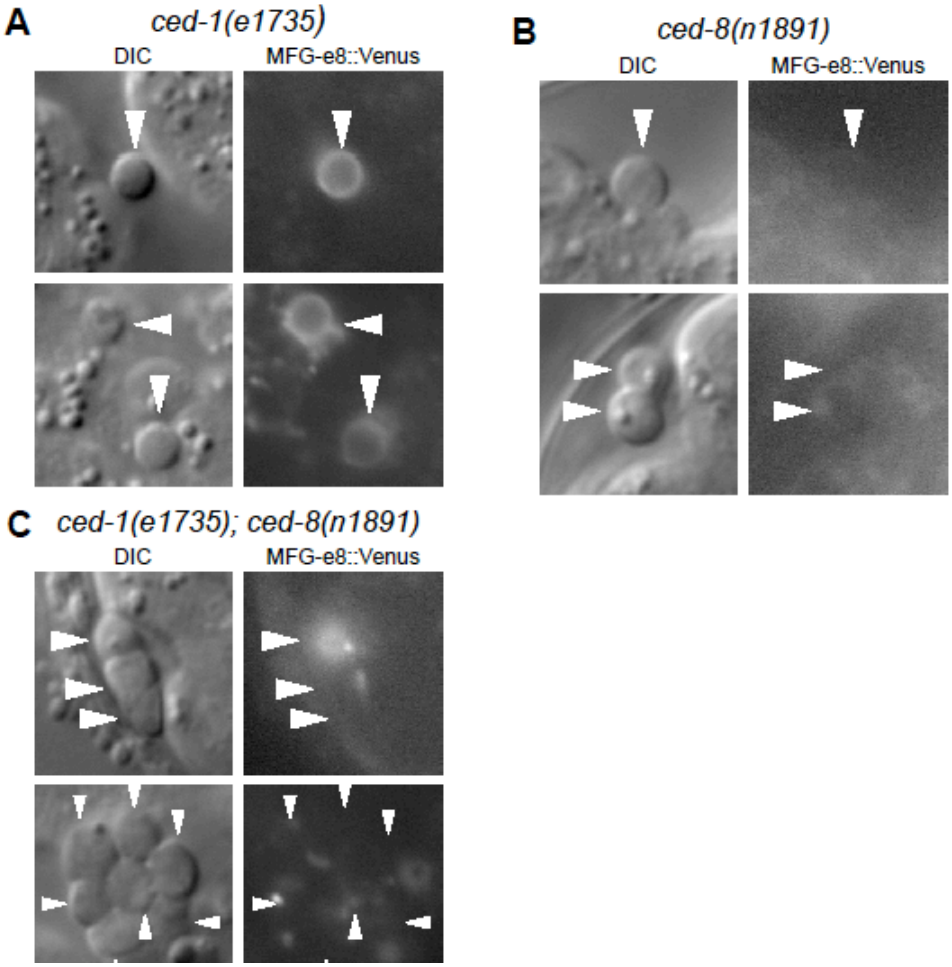

Fig. S15.

ced-8 promotes PtdSer exposure on the cell surface of floaters, the unengulfed apoptotic cell corpses that detach from engulfment-defective mutant embryos. Shown are Nomarski DIC and fluorescent micrographs of floaters (indicated by arrowheads) generated by ***(A)*** *ced-1(e1735)*, ***(B)*** *ced-8(n1891)*, and ***(C)*** *ced-1(e1735); ced-8(n1891)* mutants. PtdSer was detected using secreted MFG-e8::Venus expressed from the transgene *nIs398.* All floaters imaged were generated by embryos at the 1.5-fold stage of development or earlier. At later stages of embryonic development, *ced-8* mutant floaters exhibit some PtdSer exposure, indicating that *ced-8* mutations delay the process of PtdSer exposure and that *C. elegans* contains additional mechanisms of PtdSer exposure.

References and Notes

1. P. A. Leventis, S. Grinstein, The distribution and function of phosphatidylserine in cellular membranes. *Annu. Rev. Biophys.* **39**, 407–427 (2010). doi:10.1146/annurev.biophys.093008.131234 Medline

2. K. S. Ravichandran, U. Lorenz, Engulfment of apoptotic cells: Signals for a good meal. *Nat. Rev. Immunol.* **7**, 964–974 (2007). doi:10.1038/nri2214 Medline

3. S. Nagata, R. Hanayama, K. Kawane, Autoimmunity and the clearance of dead cells. *Cell* **140**, 619–630 (2010). doi:10.1016/j.cell.2010.02.014 Medline

4. E. M. Bevers, P. L. Williamson, Phospholipid scramblase: An update. *FEBS Lett.* **584**, 2724–2730 (2010). doi:10.1016/j.febslet.2010.03.020 Medline

5. J. Suzuki, M. Umeda, P. J. Sims, S. Nagata, Calcium-dependent phospholipid scrambling by TMEM16F. *Nature* **468**, 834–838 (2010). doi:10.1038/nature09583 Medline

6. J. Suzuki, T. Fujii, T. Imao, K. Ishihara, H. Kuba, S. Nagata, Calcium-dependent phospholipid scramblase activity of TMEM16 protein family members. *J. Biol. Chem.* **288**, 13305–13316 (2013). doi:10.1074/jbc.M113.457937 Medline

7. G. Calenda, J. Peng, C. M. Redman, Q. Sha, X. Wu, S. Lee, Identification of two new members, XPLAC and XTES, of the XK family. *Gene* **370**, 6–16 (2006). doi:10.1016/j.gene.2005.10.037 Medline

8. S. Nagata, Apoptosis by death factor. *Cell* **88**, 355–365 (1997). doi:10.1016/S0092-8674(00)81874-7 Medline

9. B. Fadeel, B. Gleiss, K. Högstrand, J. Chandra, T. Wiedmer, P. J. Sims, J. I. Henter, S. Orrenius, A. Samali, Phosphatidylserine exposure during apoptosis is a cell-type-specific event and does not correlate with plasma membrane phospholipid scramblase expression. *Biochem. Biophys. Res. Commun.* **266**, 504–511 (1999). doi:10.1006/bbrc.1999.1820 Medline

10. V. A. Fadok, A. de Cathelineau, D. L. Daleke, P. M. Henson, D. L. Bratton, Loss of phospholipid asymmetry and surface exposure of phosphatidylserine is required for phagocytosis of apoptotic cells by macrophages and fibroblasts. *J. Biol. Chem.* **276**, 1071–1077 (2001). doi:10.1074/jbc.M003649200 Medline

11. R. Hanayama, M. Tanaka, K. Miwa, A. Shinohara, A. Iwamatsu, S. Nagata, Identification of a factor that links apoptotic cells to phagocytes. *Nature* **417**, 182–187 (2002). doi:10.1038/417182a Medline

12. J. G. Herman, J. R. Graff, S. Myöhänen, B. D. Nelkin, S. B. Baylin, Methylation-specific PCR: A novel PCR assay for methylation status of CpG islands. *Proc. Natl. Acad. Sci. U.S.A.* **93**, 9821–9826 (1996). doi:10.1073/pnas.93.18.9821 Medline

13. P. Williamson, A. Christie, T. Kohlin, R. A. Schlegel, P. Comfurius, M. Harmsma, R. F. Zwaal, E. M. Bevers, Phospholipid scramblase activation pathways in lymphocytes. *Biochemistry* **40**, 8065–8072 (2001). doi:10.1021/bi001929z Medline

14. S. M. Schoenwaelder, Y. Yuan, E. C. Josefsson, M. J. White, Y. Yao, K. D. Mason, L. A. O'Reilly, K. J. Henley, A. Ono, S. Hsiao, A. Willcox, A. W. Roberts, D. C. Huang, H. H.

Salem, B. T. Kile, S. P. Jackson, Two distinct pathways regulate platelet phosphatidylserine exposure and procoagulant function. *Blood* **114**, 663–666 (2009). doi:10.1182/blood-2009-01-200345 Medline

15. G. M. Stanfield, H. R. Horvitz, The *ced-8* gene controls the timing of programmed cell deaths in *C. elegans*. *Mol. Cell* **5**, 423–433 (2000). doi:10.1016/S1097-2765(00)80437-2 Medline

16. Y. C. Wu, G. M. Stanfield, H. R. Horvitz, NUC-1, a caenorhabditis elegans DNase II homolog, functions in an intermediate step of DNA degradation during apoptosis. *Genes Dev.* **14**, 536–548 (2000). 10.1101/gad.14.5.536 Medline

17. D. P. Denning, V. Hatch, H. R. Horvitz, Programmed elimination of cells by caspase-independent cell extrusion in *C. elegans*. *Nature* **488**, 226–230 (2012). doi:10.1038/nature11240 Medline

18. V. Venegas, Z. Zhou, Two alternative mechanisms that regulate the presentation of apoptotic cell engulfment signal in *Caenorhabditis elegans*. *Mol. Biol. Cell* **18**, 3180–3192 (2007). doi:10.1091/mbc.E07-02-0138 Medline

19. D. L. Bratton, V. A. Fadok, D. A. Richter, J. M. Kailey, L. A. Guthrie, P. M. Henson, Appearance of phosphatidylserine on apoptotic cells requires calcium-mediated nonspecific flip-flop and is enhanced by loss of the aminophospholipid translocase. *J. Biol. Chem.* **272**, 26159–26165 (1997). doi:10.1074/jbc.272.42.26159 Medline

20. M. B. Hampton, D. M. Vanags, M. I. Pörn-Ares, S. Orrenius, Involvement of extracellular calcium in phosphatidylserine exposure during apoptosis. *FEBS Lett.* **399**, 277–282 (1996). doi:10.1016/S0014-5793(96)01341-5 Medline

21. L. E. Muñoz, K. Lauber, M. Schiller, A. A. Manfredi, M. Herrmann, The role of defective clearance of apoptotic cells in systemic autoimmunity. *Nat. Rev. Rheumatol.* **6**, 280–289 (2010). doi:10.1038/nrrheum.2010.46 Medline

22. A. L. Franks, J. E. Slansky, Multiple associations between a broad spectrum of autoimmune diseases, chronic inflammatory diseases and cancer. *Anticancer Res.* **32**, 1119–1136 (2012). Medline

23. J. Mapes, Y. Z. Chen, A. Kim, S. Mitani, B. H. Kang, D. Xue, CED-1, CED-7, and TTR-52 regulate surface phosphatidylserine expression on apoptotic and phagocytic cells. *Curr. Biol.* **22**, 1267–1275 (2012). doi:10.1016/j.cub.2012.05.052 Medline

24. Y. Zhang, H. Wang, E. Kage-Nakadai, S. Mitani, X. Wang, *C. elegans* secreted lipid-binding protein NRF-5 mediates PS appearance on phagocytes for cell corpse engulfment. *Curr. Biol.* **22**, 1276–1284 (2012). doi:10.1016/j.cub.2012.06.004 Medline

25. R. Palacios, M. Steinmetz, Il-3-dependent mouse clones that express B-220 surface antigen, contain Ig genes in germ-line configuration, and generate B lymphocytes in vivo. *Cell* **41**, 727–734 (1985). doi:10.1016/S0092-8674(85)80053-2 Medline

26. K. A. Tucker, M. B. Lilly, L. Heck Jr., T. A. Rado, Characterization of a new human diploid myeloid leukemia cell line (PLB-985) with granulocytic and monocytic differentiating capacity. *Blood* **70**, 372–378 (1987). Medline

27. S. Morita, T. Kojima, T. Kitamura, Plat-E: An efficient and stable system for transient packaging of retroviruses. *Gene Ther.* **7**, 1063–1066 (2000). doi:10.1038/sj.gt.3301206 Medline

28. R. Fukunaga, E. Ishizaka-Ikeda, S. Nagata, Purification and characterization of the receptor for murine granulocyte colony-stimulating factor. *J. Biol. Chem.* **265**, 14008–14015 (1990). Medline

29. T. Shiraishi, K. Suzuyama, H. Okamoto, T. Mineta, K. Tabuchi, K. Nakayama, Y. Shimizu, J. Tohma, T. Ogihara, H. Naba, H. Mochizuki, S. Nagata, Increased cytotoxicity of soluble Fas ligand by fusing isoleucine zipper motif. *Biochem. Biophys. Res. Commun.* **322**, 197–202 (2004). doi:10.1016/j.bbrc.2004.07.098 Medline

30. T. Kitamura, Y. Koshino, F. Shibata, T. Oki, H. Nakajima, T. Nosaka, H. Kumagai, Retrovirus-mediated gene transfer and expression cloning: Powerful tools in functional genomics. *Exp. Hematol.* **31**, 1007–1014 (2003). 10.1016/j.exphem.2003.07.005 Medline

31. R. Higuchi, in *PCR Protocols: A Guide to Methods and Applications* (Academic Press, San Diego, 1990), pp. 177–188.

32. F. Köntgen, G. Süss, C. Stewart, M. Steinmetz, H. Bluethmann, Targeted disruption of the MHC class II Aa gene in C57BL/6 mice. *Int. Immunol.* **5**, 957–964 (1993). doi:10.1093/intimm/5.8.957 Medline

33. K. Sakai, J. i. Miyazaki, A transgenic mouse line that retains Cre recombinase activity in mature oocytes irrespective of the cre transgene transmission. *Biochem. Biophys. Res. Commun.* **237**, 318–324 (1997). doi:10.1006/bbrc.1997.7111 Medline

34. H. Kanki, H. Suzuki, S. Itohara, High-efficiency CAG-FLPe deleter mice in C57BL/6J background. *Exp. Anim.* **55**, 137–141 (2006). doi:10.1538/expanim.55.137 Medline

35. J. A. Cattermole, P. S. Crosier, E. Leung, R. W. Overell, S. Gillis, J. D. Watson, Isolation of murine fetal thymus cell lines after infection with recombinant retroviruses containing the v-myc and v-Ha-ras oncogenes. *J. Immunol.* **142**, 3746–3753 (1989). Medline

36. T. Imao, S. Nagata, Apaf-1- and caspase-8-independent apoptosis. *Cell Death Differ.* **20**, 343–352 (2013). doi:10.1038/cdd.2012.149 Medline

37. T. Akagi, K. Sasai, H. Hanafusa, Refractory nature of normal human diploid fibroblasts with respect to oncogene-mediated transformation. *Proc. Natl. Acad. Sci. U.S.A.* **100**, 13567–13572 (2003). doi:10.1073/pnas.1834876100 Medline

38. J. D. Watson, P. J. Morrissey, A. E. Namen, P. J. Conlon, M. B. Widmer, Effect of IL-7 on the growth of fetal thymocytes in culture. *J. Immunol.* **143**, 1215–1222 (1989). Medline

39. R. Watanabe-Fukunaga, C. I. Brannan, N. Itoh, S. Yonehara, N. G. Copeland, N. A. Jenkins, S. Nagata, The cDNA structure, expression, and chromosomal assignment of the mouse Fas antigen. *J. Immunol.* **148**, 1274–1279 (1992). Medline

40. J. Ogasawara, R. Watanabe-Fukunaga, M. Adachi, A. Matsuzawa, T. Kasugai, Y. Kitamura, N. Itoh, T. Suda, S. Nagata, Lethal effect of the anti-Fas antibody in mice. *Nature* **364**, 806–809 (1993). doi:10.1038/364806a0 Medline

41. M. Tanaka, T. Suda, T. Takahashi, S. Nagata, Expression of the functional soluble form of human fas ligand in activated lymphocytes. *EMBO J.* **14**, 1129–1135 (1995). Medline

42. Y. Aoki, T. Uenaka, J. Aoki, M. Umeda, K. Inoue, A novel peptide probe for studying the transbilayer movement of phosphatidylethanolamine. *J. Biochem.* **116**, 291–297 (1994). Medline

43. S. Toda, R. Hanayama, S. Nagata, Two-step engulfment of apoptotic cells. *Mol. Cell. Biol.* **32**, 118–125 (2012). doi:10.1128/MCB.05993-11 Medline

44. S. Brenner, The genetics of *Caenorhabditis elegans*. *Genetics* **77**, 71–94 (1974). Medline